

# Supplementary Materials

## Phase Sequence in Diisopropylammonium Iodide: Avoided Ferroelectricity by the Appearance of a Reconstructed Phase.

Anna Piecha-Bisiorek,<sup>§\*</sup> Anna Gaĝor,<sup>†</sup> Dymitry Isakov,<sup>||,‡</sup> Piotr Zieliński,<sup>††</sup> Mirosław Gałazka,<sup>††</sup> Ryszard Jakubas<sup>§</sup>

<sup>§</sup>Faculty of Chemistry, University of Wrocław, F. Joliot-Curie 14, 50-383 Wrocław, Poland.

<sup>†</sup>W. Trzebiatowski Institute of Low Temperature and Structure Research PAS, P.O. Box 1410, 50-950 Wrocław, Poland

<sup>||</sup>University of Minho, Centre of Physics, Campus de Gualtar, 4710-057 Braga, Portugal

<sup>‡</sup>University of Oxford, Department of Materials, Parks Road, Oxford OX1 3PH, United Kingdom

<sup>††</sup>The H. Niewodniczański Institute of Nuclear Physics, PAS, Radzikowskiego 152, 31-342 Kraków, Poland.

e-mail: [anna.piecha@chem.uni.wroc.pl](mailto:anna.piecha@chem.uni.wroc.pl)

### TABLE OF CONTENTS:

1. Thermal properties (TGA-DTA)
2. Crystal structure determination
3. Dielectric properties
4. Optical properties
5. Phenomenological theory of the phase transition

## Part 1

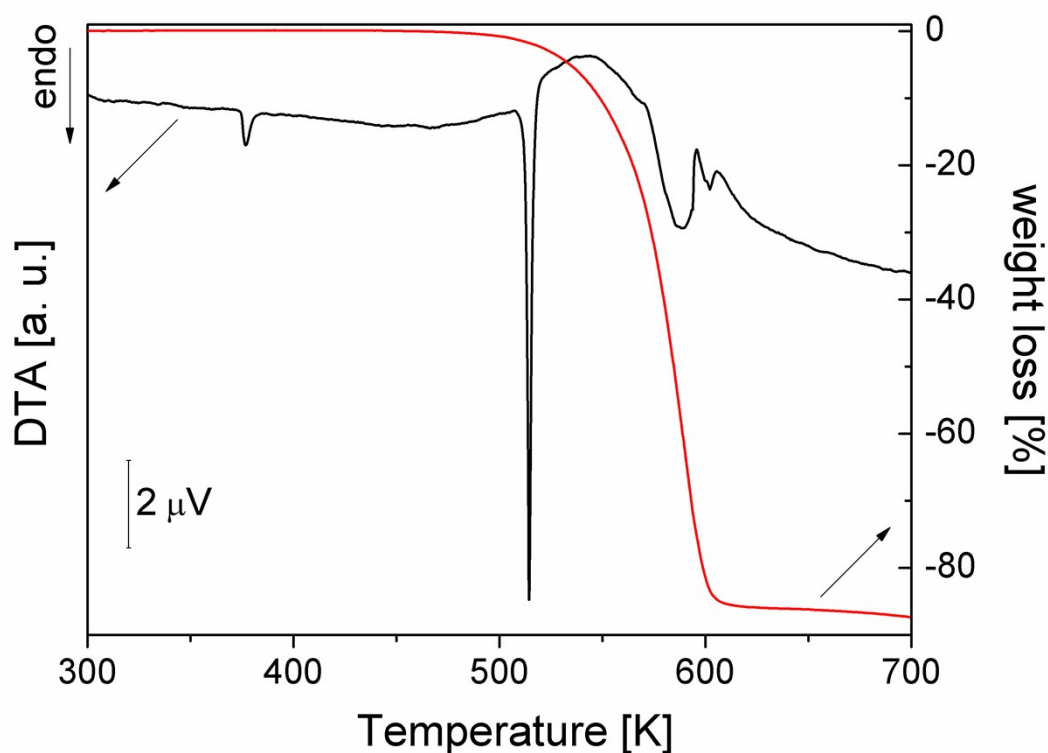


**Figure S1.** Simultaneous TGA and DTA thermograms between 300 and 700 K for DIPAI

## Part 2

For all structures:  $C_6H_{16}IN$ ,  $M_r = 229.10$ . Experiments were carried out with Mo  $K\alpha$  radiation using a Xcalibur, Sapphire1. Absorption was corrected by multi-scan methods, *CrysAlis RED*, Oxford Diffraction Ltd., Version 1.171.33.42 (release 29-05-2009 *CrysAlis171 .NET*) (compiled May 29 2009,17:40:42) Empirical absorption correction using spherical harmonics, implemented in SCALE3 ABSPACK scaling algorithm.

Table S1. Experimental details

	Phase III	Phase I
<i>Crystal data</i>		
Crystal system, space group	Orthorhombic, $P2_12_12_1$	Monoclinic, $P2_1/m$
Temperature (K)	295	405
$a, b, c$ (Å)	8.3519 (1), 8.3673 (2), 14.2217 (3)	8.291 (2), 8.367 (2), 8.309 (2)
$\alpha, \beta, \gamma$ (°)	90, 90, 90	90, 118.95 (1), 90
$V$ (Å <sup>3</sup> )	993.85 (3)	504.4 (2)
$Z$	4	2
$\mu$ (mm <sup>-1</sup> )	3.15	3.10
Crystal size (mm)	0.21 × 0.15 × 0.13	0.21 × 0.15 × 0.13
<i>Data collection</i>		
$T_{\min}, T_{\max}$	0.882, 1.000	0.689, 1.000
No. of measured, independent and observed [ $I > 2\sigma(I)$ ] reflections	11297, 1891, 1348	5046, 1018, 422
$R_{\text{int}}$	0.038	0.050
$(\sin \Theta/\lambda)_{\text{max}}$ (Å <sup>-1</sup> )	0.610	0.610
<i>Refinement</i>		
$R[F^2 > 2\sigma(F^2)], wR(F^2), S$	0.024, 0.053, 0.93	0.055, 0.155, 0.81
No. of reflections	1891	1018
No. of parameters	90	37
No. of restraints	2	15
H-atom treatment	H atoms treated by a mixture of independent and constrained refinement	H-atom parameters constrained
$\Delta\rho_{\text{max}}, \Delta\rho_{\text{min}}$ (e Å <sup>-3</sup> )	0.48, -0.46	0.54, -0.62
Absolute structure	Flack $x$ determined using 483 quotients [( $I^+$ )-( $I^-$ )]/[( $I^+$ )+( $I^-$ )] (Parsons, Flack and Wagner, Acta Cryst. B69 (2013) 249-259).	–
Absolute structure parameter	-0.06 (3)	–

Computer programs: *CrysAlis CCD*, Oxford Diffraction Ltd., Version 1.171.33.42 (release 29-05-2009) *CrysAlis171 .NET* (compiled May 29 2009, 17:40:42), *CrysAlis RED*, *SHELXL2014/7* (Sheldrick, 2014).

Table S2. Selected geometric parameters (Å, °)

Phase III			
N1—C4	1.509 (10)	C1—C2	1.505 (11)
N1—C1	1.506 (9)	C4—C5	1.513 (10)
C1—C3	1.496 (12)	C4—C6	1.520 (12)
C4—N1—C1	119.4 (7)	N1—C4—C5	109.6 (7)
C3—C1—C2	113.0 (8)	N1—C4—C6	109.0 (7)
C3—C1—N1	111.2 (7)	C5—C4—C6	112.2 (7)
C2—C1—N1	108.1 (7)		
Phase I			
C4—N1	1.441 (5)	C3—C1	1.528 (6)
C4—C6	1.453 (6)	C1—N1	1.487 (5)
C4—C5	1.475 (5)	C1—C2	1.501 (6)
N1—C4—C6	121.9 (3)	N1—C4—C5	117.9 (5)
N1 <sup>i</sup> —C4—C6 <sup>i</sup>	121.9 (3)	C6—C4—C5	119.6 (4)

Symmetry code(s): (i)  $x, -y+1/2, z$ .

Table S3. Selected hydrogen-bond parameters

$D-H\cdots A$	$D-H$ (Å)	$H\cdots A$ (Å)	$D\cdots A$ (Å)	$D-H\cdots A$ (°)
Phase III				
N1—H1B $\cdots$ I1 <sup>i</sup>	0.77 (7)	2.81 (7)	3.577 (6)	176 (7)
N1—H1A $\cdots$ I1 <sup>ii</sup>	0.92 (7)	2.67 (7)	3.586 (7)	179 (6)
Phase I				
N1—H1A $\cdots$ I1	0.89	2.82	3.629 (6)	152.5
N1—H1B $\cdots$ I1 <sup>iii</sup>	0.89	3.03	3.850 (4)	153.7

Symmetry code(s): (i)  $x+1/2, -y+3/2, -z+2$ ; (ii)  $x+1, y, z$ ; (iii)  $-x+1, -y+1, -z+1$ .

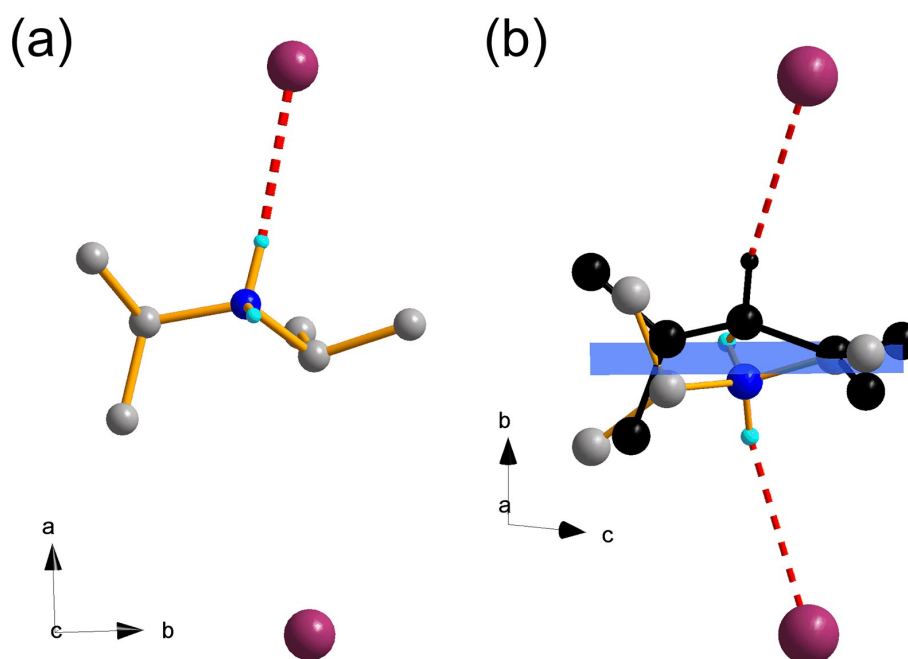


**Figure S2.** (a) The spatial arrangement of diisopropylammonium counterion in phase III, T=295 K (b) the model of disorder in the high-temperature phase I, T=405 K.

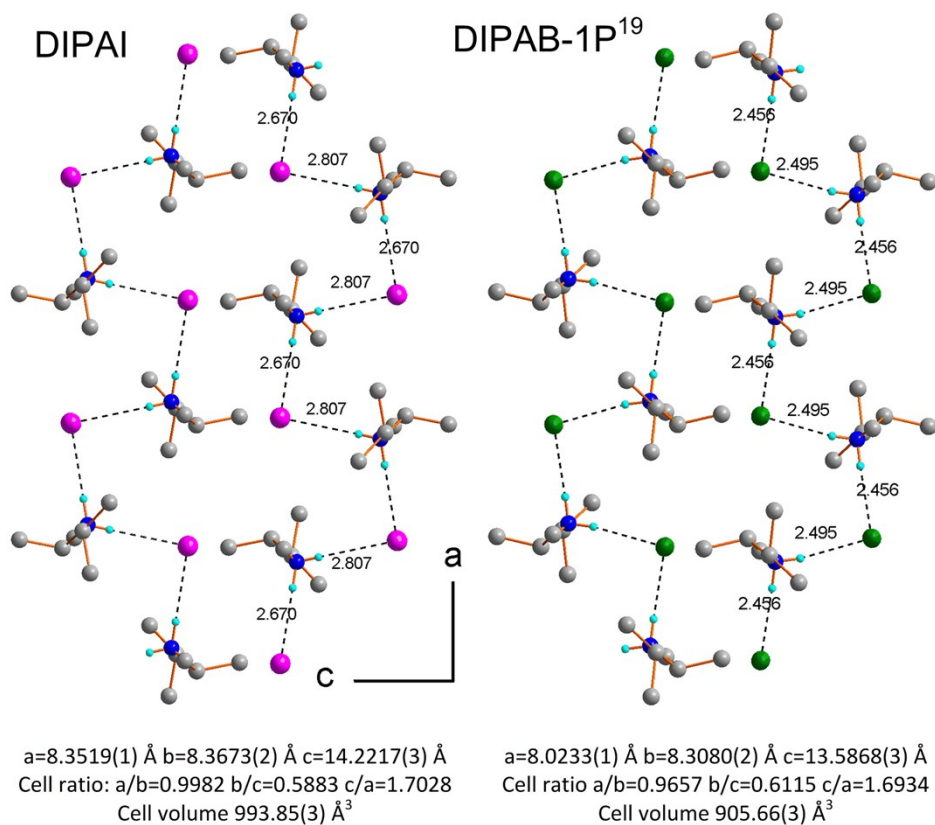


**Figure S3.** Crystal packing of DIPA isomorphs at room temperature, in the orthorhombic  $P2_12_12_1$  space group

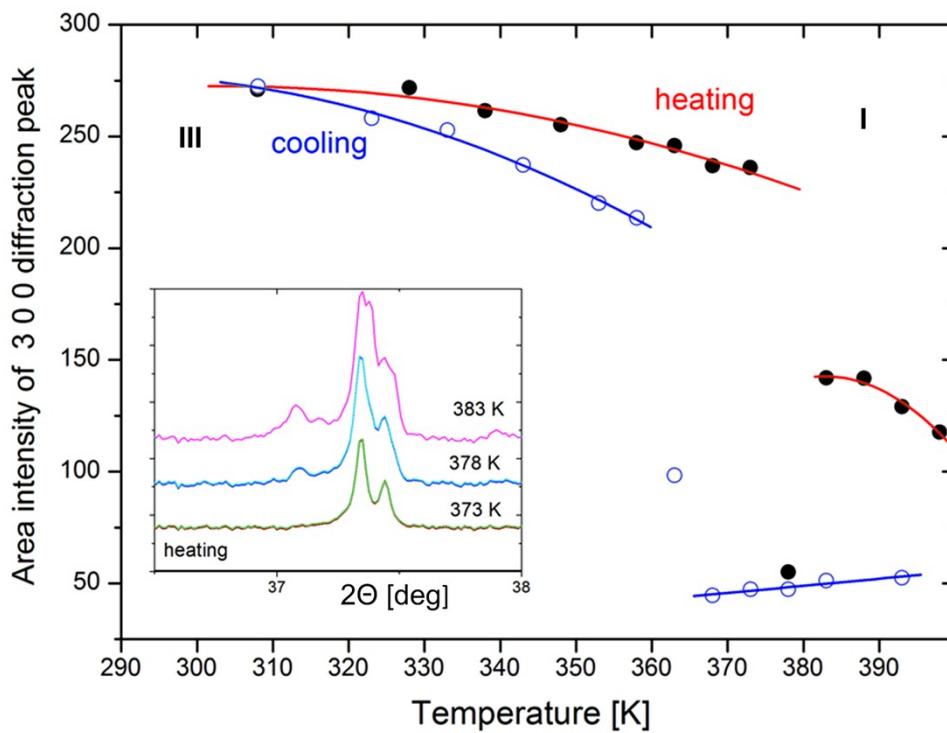


**Figure S4.** Thermal evolution of the area intensity of the 300 diffraction peak in DIPAI. At 378 K (in the heating cycle) there is phase coexistence.

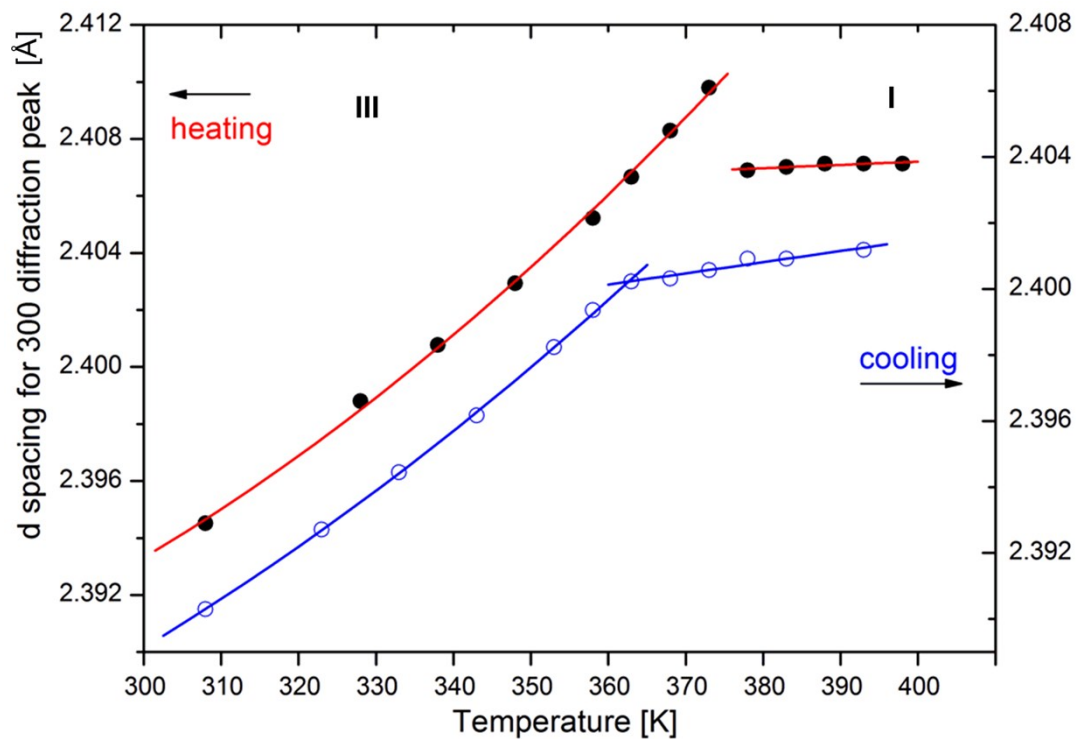


**Figure S5.** Thermal evolution of  $d_{300}$  spacing in DPAI

[1] a) H. D. Megaw, *Nature* 1945, 155, 484 – 485; b) B. Jaffe, R. S. Roth, S. Marzullo, *J. Appl. Phys.* 1954, 25, 809 – 810; c) C. Y. Chao, Z. H. Ren, Y. H. Zhu, Z. Xiao, Z. Y. Liu, G. Xu, J. Q. Mai, X. Li, G. Shen, G. R. Han, *Angew. Chem.* 2012, 124, 9417 – 9421; *Angew. Chem. Int. Ed.* 2012, 51, 9283 – 9287; d) E. J. Kan, H. J. Xiang, C. H. Lee, F. Wu, J. L. Y., M.-H. Whangbo, *Angew. Chem.* 2010, 122, 1647 – 1650; *Angew. Chem. Int. Ed.* 2010, 49, 1603 – 1606.

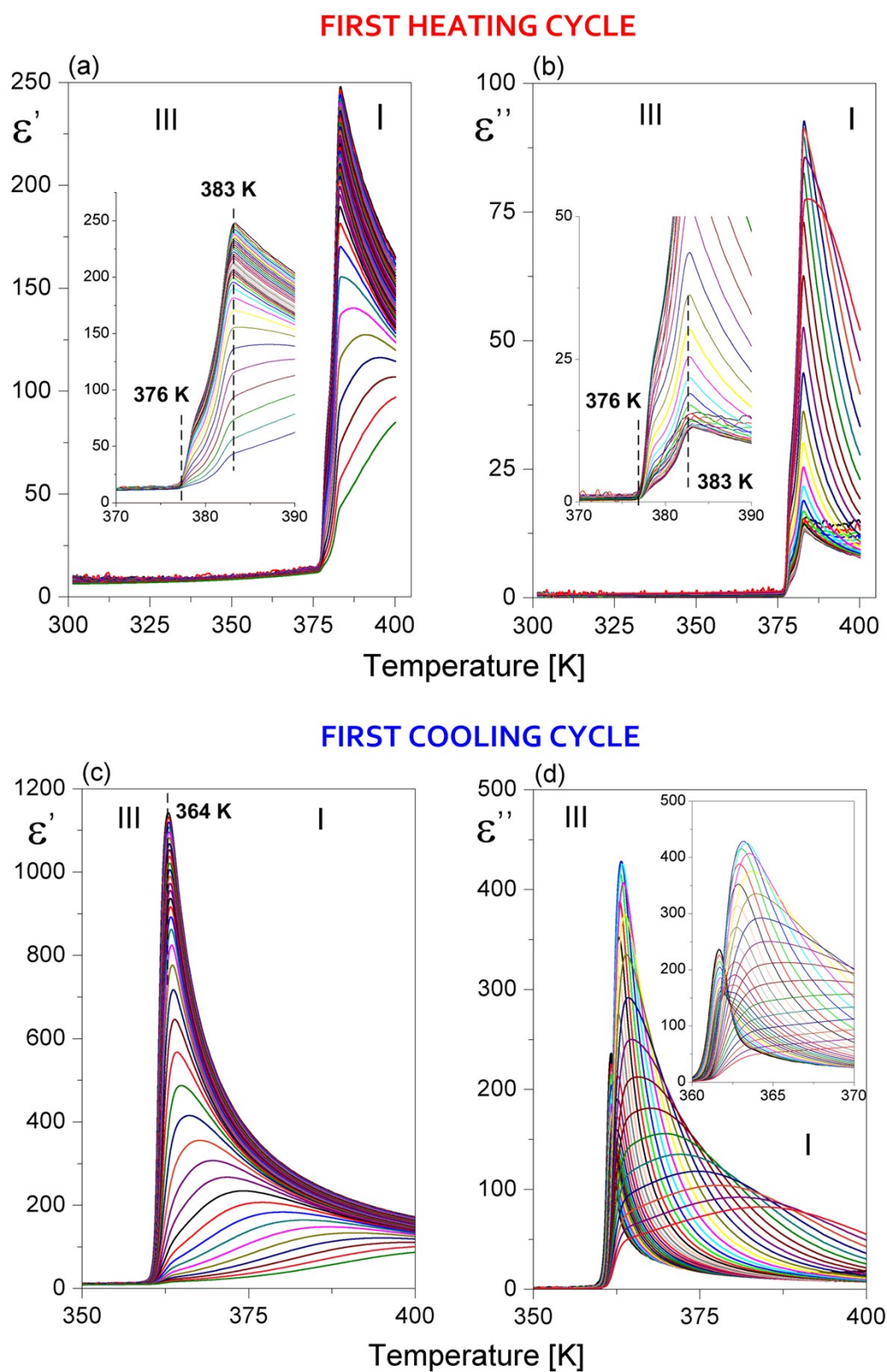
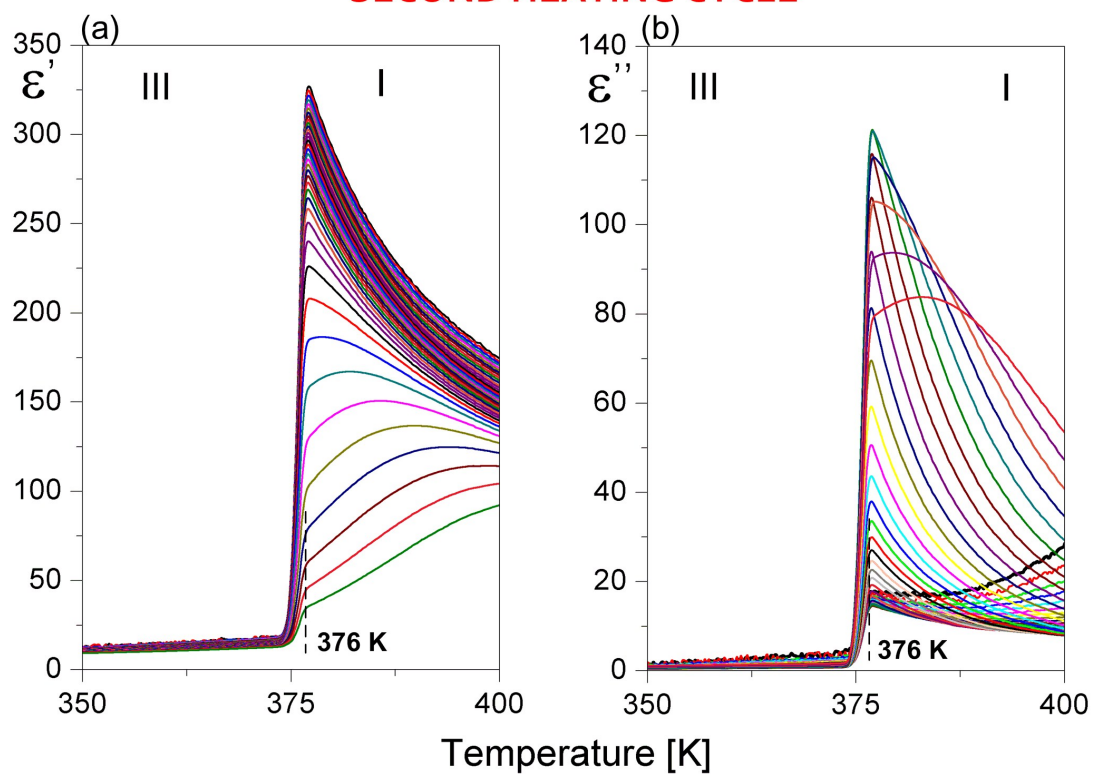


**Figure S6.** Temperature dependence of the real (a)(c) and imaginary (b)(d) parts of complex electric permittivity along the  $a$ -axis for DIPAI.

## SECOND HEATING CYCLE



## SECOND COOLING CYCLE

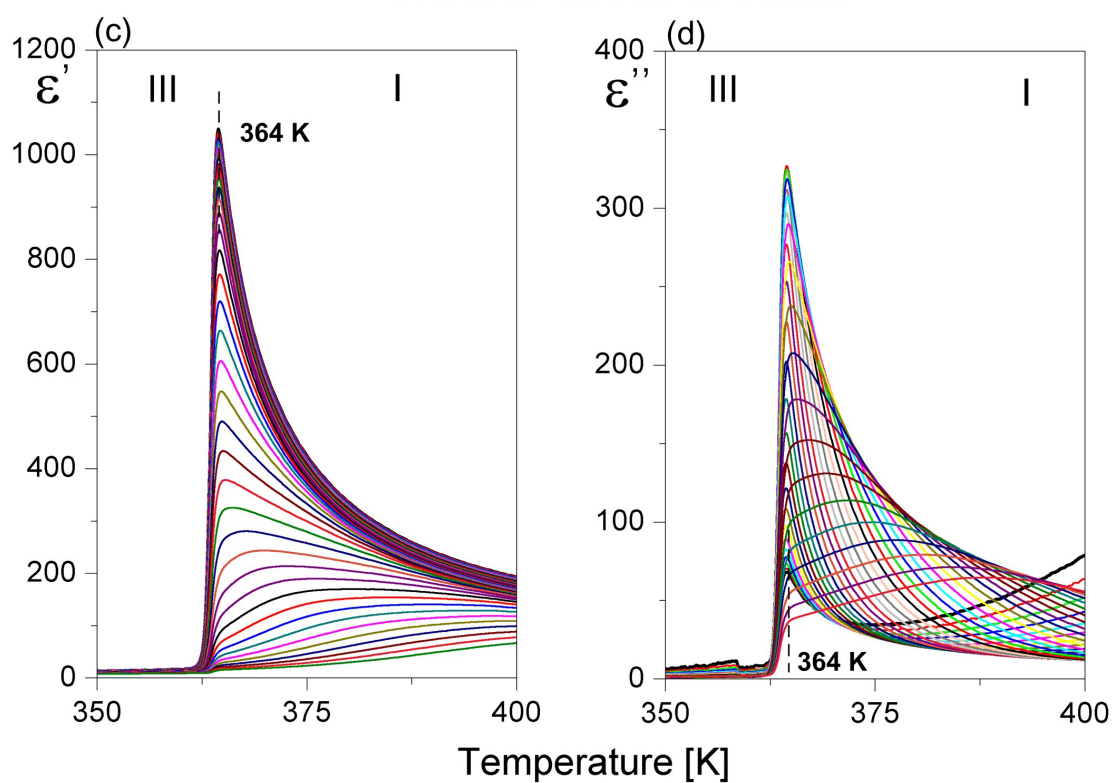


**Figure S7.** Temperature dependence of the real (a)(c) and imaginary (b)(d) parts of complex electric permittivity along the *a*-axis for DIPAI.

The results shown in Figures 2(b) are replotted in Figure 3 as  $\epsilon''$  vs.  $\epsilon'$  (Cole–Cole plot). The values of the complex dielectric constant,  $\epsilon^*$ , has been fitted with the Cole–Cole relation:

$$\epsilon^* = \epsilon_\infty + \frac{\epsilon_0 - \epsilon_\infty}{1 + (i\omega\tau)^{(1-\alpha)}} \quad (\text{S1})$$

in eq. S1  $\epsilon_0$  and  $\epsilon_\infty$  denote the low and high frequency limits of the dielectric permittivity, respectively,  $\omega$  denotes the angular frequency,  $\tau$  is the macroscopic dielectric relaxation time, while the parameter  $\alpha$  represents a measure of distribution of the relaxation times.

The parameter  $\alpha$  is approximately constant over the phase I changing between 0.07 to 0.09 when approaching  $T_c$  from above. It indicates a weakly polydispersive process. Figure S8(a) shows the temperature dependence of the characteristic relaxation time,  $\tau$ , over the phase III. It should be noticed that the dielectric process in the DIPAI crystal is characterized by an apparent critical slowing down in the vicinity of  $T_c$ . The relaxation time,  $\tau$ , fulfils quite well the Curie–Weiss behaviour,  $\tau \propto (T - T_c)^{-1}$ , as shown in Figure S8(a).

It should be stressed, however, that for ferroelectrics with the order–disorder mechanism of the phase transition the dynamics of the dielectric relaxator may be described by the microscopic relaxation time,  $\tau_0$ , defined as:

$$\tau_0 = \tau \frac{\epsilon_\infty}{\epsilon_0 - \epsilon_\infty} \quad (\text{S2})$$

Then, the activation energy  $E_a$  may be calculated according to the modified Arrhenius equation (usually valid for ferroelectrics) where  $h$  and  $k_B$  are Plank and Boltzmann constants, respectively. [2]

$$\tau_0 = \left( \frac{h}{k_B T} \right) \exp \left( \frac{E_a}{k_B T} \right) \quad (\text{S3})$$

The  $E_a$  (see Figure S8(b)) estimated from the eq. S3 is quite large and characteristic of bulky dipoles performing the reorientational motion.

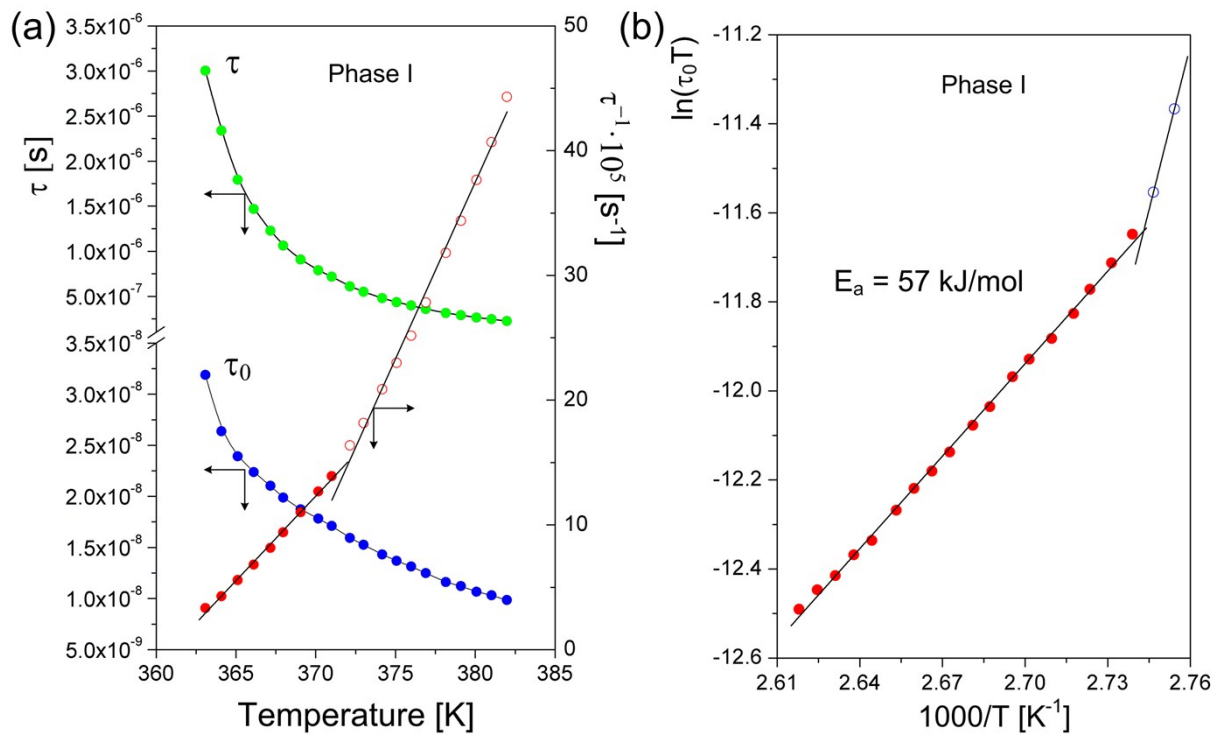


**Figure S8.** (a) Temperature dependence of the main relaxation time,  $\tau$ , its inverse  $\tau^{-1}$  and  $\tau_0$  (b) Activation energy ( $E_a$ ) for DIPAI in the vicinity of the phase transition obtained by means of the modified Arrhenius equation (eq. 3)

Part 4

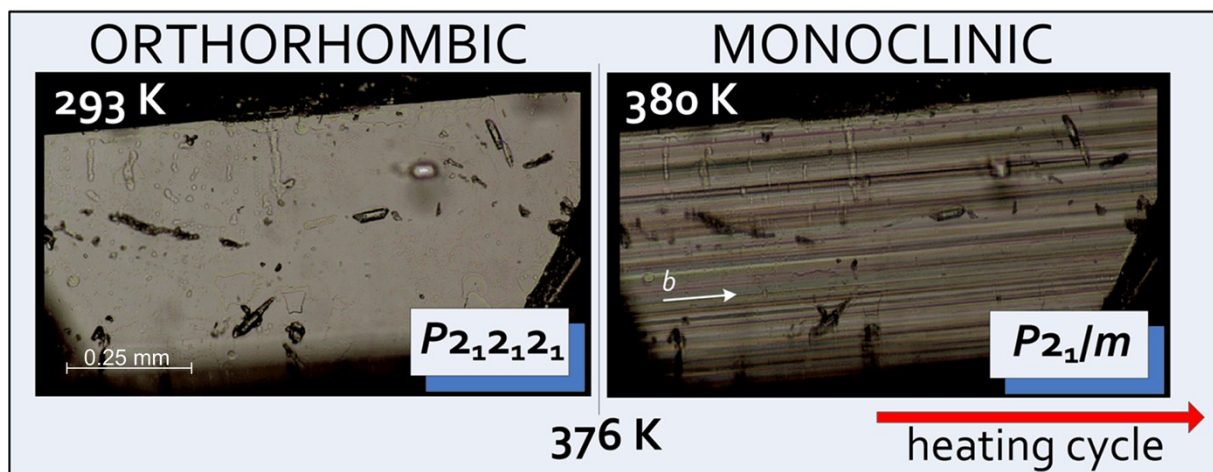


**Figure S9.** Evolution of the domain pattern during heating of the DIPAI sample

[2] J. Grigas, Microwave Dielectric Spectroscopy of Ferroelectrics and Related Materials; Ferroelectricity and Related Phenomena, Vol. 9, Gordon and Breach Publishers: The Netherlands, 1996.

## Part 5

The simplest *Cmcm* invariant expansion of the free energy that describes the sequence of the phase transitions in DIPAB, DIPAC and DIPAI reads:

$$\begin{aligned}
 F = F_0 + \frac{A_1}{2}\eta_1^2 + \frac{B_1}{4}\eta_1^4 \\
 + \frac{A_2}{2}\eta_2^2 + \frac{B_2}{4}\eta_2^4 + \frac{C}{2}\eta_2^2\eta_3^2 \\
 + \frac{A_3}{2}\eta_3^2 + \frac{B_3}{4}\eta_3^4.
 \end{aligned} \tag{S4}$$

For the global stability the fourth order coefficients must satisfy the following conditions

$$B_2 > 0, \quad B_3 > 0, \quad \text{and} \quad B_2B_3 - C^2 > 0. \tag{S5}$$

As it is the case in the typical Landau type theories we ascribe a temperature dependence to the coefficients  $A_1, A_2$  and  $A_3$ . Having no experimental data on the thermal evolution of the order parameter  $\eta_1$  we can also put the coefficient  $A_1$  a negative constant and assume that the initial phase I corresponds to a minimum of the free energy at  $(\bar{\eta}_1, 0, 0)$  (the overbar denotes the spontaneous value of the corresponding order parameter). For the sake of simplicity we assume that the value of the free energy at this point is equal to zero, i.e.

$$F_0 + \frac{A_1}{2}\bar{\eta}_1^2 + \frac{B_1}{4}\bar{\eta}_1^4 = 0.$$

The phase transition to the ferroelectric phase II corresponds to the appearance of the spontaneous polarization  $\eta_3$  by crossing a critical temperature  $T_c$  so that  $A_3 = a_3(T - T_c)$ .

The phase III is situated in a different location of the order parameter space. It namely corresponds to the point

$$\begin{aligned}
 \bar{\eta}_2^2 &= -(B_3A_2 - CA_3) / (B_2B_3 - C^2) \\
 \bar{\eta}_3^2 &= -(B_2A_3 - CA_2) / (B_2B_3 - C^2),
 \end{aligned} \tag{S6}$$

which describes an extremum of the free energy provided both r.h.s. be positive.

In the case of the DIPAI the phase II does not occur. This means that the minimum of the free energy with the order parameters given in Eq. (S6) becomes deeper, i.e.  $F(0, \bar{\eta}_2, \bar{\eta}_3) < 0$ , with still  $A_3 = a_3(T - T_c) > 0$ . This requires a temperature dependence of the coefficient  $A_2$ .

One can easily check that the value of this coefficient, necessarily negative, corresponding to  $F(\bar{\eta}_1, 0, \bar{\eta}_3) = 0$ , i.e. the phase equilibrium between the phases I and III is given by the following formula

$$A_2^{I-III} = \frac{CA_3}{B_3} - \frac{\sqrt{(B_2B_3 - C^2)(F_0B_3 - A_3^2)}}{B_3}. \quad (S7)$$

Analogous formula for the equilibrium of phases II and III occurring in other members of the family is obtained by equating  $F(\bar{\eta}_1, 0, \bar{\eta}_3) = -\frac{A_3^2}{4B_3}$ . The respective value formula reads

$$A_2^{II-III} = \frac{CA_3}{B_3} - \frac{\sqrt{(B_2B_3 - C^2)(4F_0B_3 - 3A_3^2)}}{2B_3}. \quad (S8).$$

The present model describes correctly the behavior of the electric susceptibility in phase I, see Figure S10

$$\chi(T) = 1/A_3 = \frac{1}{a_3(T - T_c)}. \quad (S9)$$

The susceptibility grows with decreasing temperature but does not reach infinity. The temperature dependence of  $A_2$  can be, in principle, fitted to the experimental temperature dependence of the superstructure reflections intensity due to the unit cell doubling. Such temperature-dependent crystallographic data are not available for the moment.

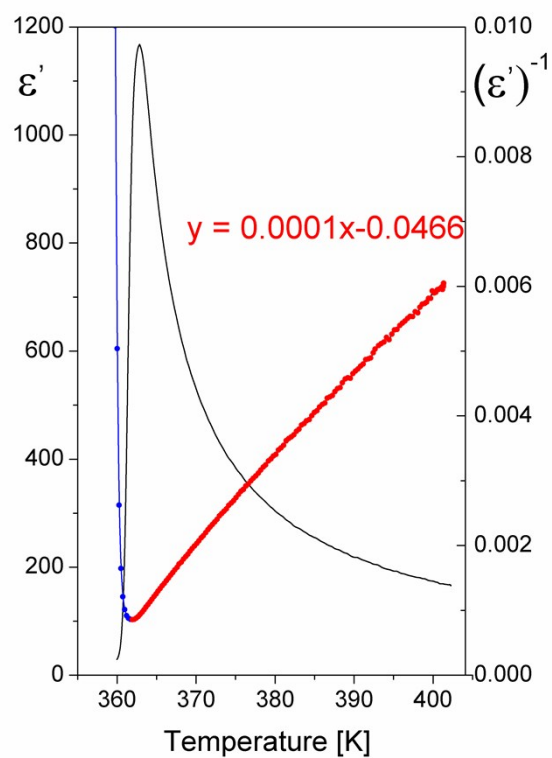


**Figure S10.** Low frequency electric permittivity in DIPAI and its inverse showing the behaviour consistent with eq. (S9).